JOURNAL OF SPACECRAFT AND ROCKETS
Vol. 32, No. 1, January–February 1995

Roe's Solver with Different Turbulence Models for Three-Dimensional High-Speed Inlets

Chang-Hsien Tai,* Jiann-Hwa Sheu,† and Shian-Chung Tzeng‡
Chung Cheng Institute of Technology, Ta-Shi, Taoyuan, Taiwan, Republic of China

A high-resolution Roe's solver combined with different turbulence models is used to simulate the flowfield of a high-speed inlet that is characterized by the complex phenomena of oblique-shock-wave–boundary-layer interaction and interaction between oblique shock waves. The wall effect in a real three-dimensional flowfield is also considered. Fairly good agreement is obtained by comparing the numerical results of the turbulent simulation with experimental data. It is found that the Mitcheltree one-equation model is more reliable than the others. The one-equation model can also be used in simulating the high-speed inlet flow with the good accuracy.

Nomenclature

C_p	= pressure coefficient, $(P - P_\infty)/(\rho_\infty V_\infty^2/2)$
E	= total energy, J/kg
$\boldsymbol{F}, \boldsymbol{G}, \boldsymbol{H}$	= flux vectors in x, y, and z directions
H^*	= total enthalpy, J/kg
M	= Mach number
P	= pressure, N/m^2
Pr	= Prandtl number
q	= heat conduction, J/m^2-s
Re	= Reynolds number
T	= temperature, K
t	= time, s
$\boldsymbol{U}$	= vector of the conservative variables
u, v, w	= velocity components in x, y, and z directions, m/s
V	= velocity, m/s
X, Y, Z	= Cartesian coordinates, in.
x, y, z	= Cartesian coordinates, m
ΔA_n	= dimensionless area of nth face of a hexahedral cell
$\Delta \tilde{V}$	= dimensionless volume of hexahedral cell
μ	= coefficient of viscosity, kg/m-s
ρ	= density, kg/m^2
τ	= shear stress, N/m^2

Subscripts and Superscripts

i	= inviscid part
lam	= laminar flow
n	= nth face of hexahedral cell
t	= turbulent flow
∞	= inlet condition
μ	= viscous part

Introduction

ATMOSPHERIC engine performance depends greatly on the inlet design. High-pressure recovery requirements are pertinent to high-speed inlets when aircraft are flying in the supersonic region. The shock waves caused by successive compression waves play an important role in providing pressure recovery. Inside the inlet duct the complex shock acts on the boundary layer and results in an adverse pressure gradient with respect to the flow convecting downstream. Under that pressure gradient, the boundary-layer thickness will grow rapidly and can ultimately cause the formation of a flow separation region. The temperature within this region may also rise, especially at high Mach numbers. Once the temperature grows beyond the limits of the material endurance, many interrelated problems will result. To prevent this situation, it is essential to be able to predict correctly the location, strength, and shape of the shock, and the location of the separation region. In order to predict the complex physical phenomena of the entire inlet flowfield, it is necessary to investigate the accuracy of different turbulence models.[1]

Research on this problem has been progressing. In 1965, a calculation of the axisymmetric inlet flowfield using the method of characteristics was first made by Sorensen.[2] Later, in 1982, a three-dimensional inlet field was analyzed by Vadyak and Hoffman[3] using a method combining inviscid and viscous interaction to treat the oblique-shock–boundary-layer interaction region. Recently, the work of Darian and Daso[4] used a finite-volume code to analyze shock-interaction flow structures in high-speed inlets. They employ a highly accurate total-variation-diminishing formulation and Roe's approximate Riemann solver to compute the fluxes. Based on these computational results, it seems that the algebraic turbulence model cannot be used to simulate the flowfield very well. According to the above literature review, it is clear that different turbulence models need to be tested and three-dimensional effects should be included. In this paper, an improved numerical approach is made to simulate the high-speed inlet flowfield. An explicit multistage upwind flux-difference split scheme (Roe's scheme), coupled with different turbulence models including the Baldwin-Lomax algebraic model,[5] the Mitcheltree one-equation model,[6] and the Launder-Sharma k-ε two-equation model,[7] has been developed to solve the steady Reynolds-averaged Navier-Stokes equations. To validate the code, a two-dimensional viscous flowfield analysis characterized by the complex phenomena of oblique-shock-wave–boundary-layer interaction and interaction between oblique shock waves was conducted. Comparing the results with experimental data, one finds fairly good agreement for the application of each of the different turbulence models mentioned. However, the accuracy of Mitcheltree's one-equation model is superior to the others. Finally, the same numerical method was applied to simulate a three-dimensional high-speed mixed compression inlet flowfield.

Computational Grid

Because of the complexity of the oblique-shock-wave–boundary-layer interaction region, it is necessary to allocate stretching grids in that region. Algebraically spaced grids are used to cover the flowfield, and the stretching transformation clusters are made near the boundary layer, using the Roberts[8] generalized stretching transformation technique. The multiblock grid approach is used in this study. The total number of cells is 29×93 plus 245×64 plus 122×29 with respect to the two-dimensional plate partitioned as shown in Fig. 1. The total number of cells for the three-dimensional inlet flowfield

Received March 19, 1993; revision received Sept. 1, 1993; accepted for publication April 1, 1994.

*Associate Professor, Department of Mechanical Engineering.
†Ph.D. Candidate, Department of Weapon System Engineering.
‡Graduate Research Assistant, Department of Weapon System Engineering.

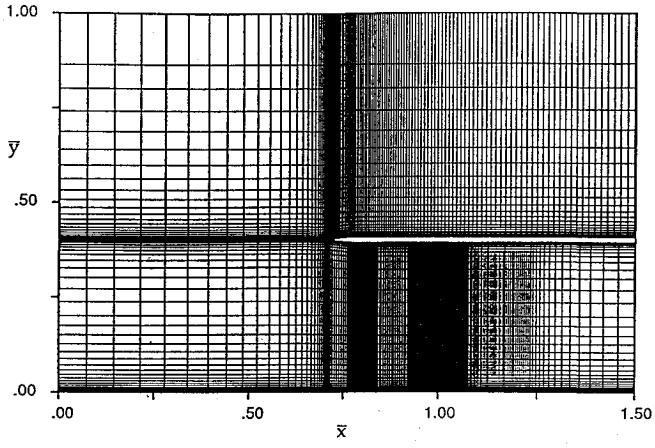

Fig. 1 Computational mesh for two-dimensional plate.

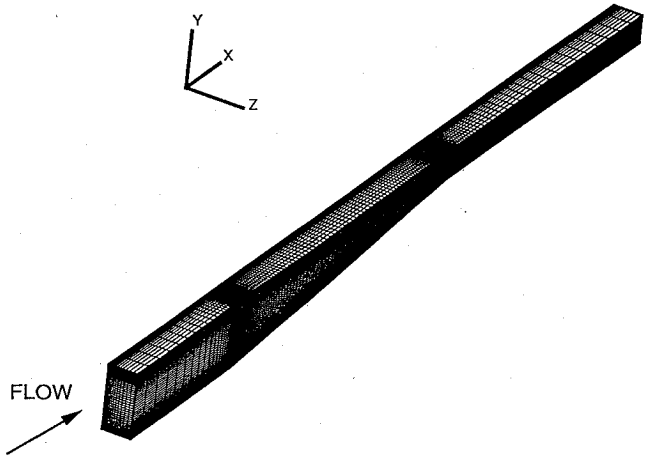

Fig. 2 Coordinate system and computational mesh for three-dimensional inlet.

(with a single-block grid) is 194 × 74 × 19, as shown in Fig. 2. The finest cell of both grids was about 5.0×10^{-4} in the x direction and 5.0×10^{-5} in the y direction.

The steady-state solutions were obtained by resolving the time-dependent governing equations, and measured by the order of magnitude of the decay in the residual (L_1 norm). The solutions were considered converged when the residual had decayed by about 5 orders of magnitudes. Computation was performed on finer and coarser grids for a grid resolution study; it was found that the total grid sizes, especially in the y direction, depend on the turbulence models used. The total grid sizes selected were chosen for suitability in comparing the accuracy of different turbulence models.

Governing Equations

The three-dimensional Reynolds-averaged Navier-Stokes governing equation can be rewritten in a strong conservation form as

$$\frac{\partial \boldsymbol{U}}{\partial t} + \frac{\partial \boldsymbol{F}}{\partial x} + \frac{\partial \boldsymbol{G}}{\partial y} + \frac{\partial \boldsymbol{H}}{\partial z} = 0 \tag{1}$$

where x is the streamwise direction, and

$$\boldsymbol{U} = \begin{bmatrix} \rho \\ \rho u \\ \rho v \\ \rho w \\ \rho E \end{bmatrix}, \quad \boldsymbol{F} = \begin{bmatrix} \rho u \\ \rho u^2 + P - \tau_{xx} \\ \rho uv - \tau_{xy} \\ \rho uw - \tau_{xz} \\ \rho u H^* - u\tau_{xx} - v\tau_{xy} - w\tau_{xz} + q_x \end{bmatrix}$$

$$\boldsymbol{G} = \begin{bmatrix} \rho v \\ \rho uv - \tau_{xy} \\ \rho v^2 + P - \tau_{yy} \\ \rho vw - \tau_{yz} \\ \rho v H^* - u\tau_{xy} - v\tau_{yy} - w\tau_{yz} + q_y \end{bmatrix}$$

$$\boldsymbol{H} = \begin{bmatrix} \rho w \\ \rho uw - \tau_{xz} \\ \rho vw - \tau_{yz} \\ \rho w^2 + P - \tau_{zz} \\ \rho w H^* - u\tau_{xz} - v\tau_{yz} - w\tau_{zz} + q_z \end{bmatrix}$$

where the viscous stresses and the heat fluxes are defined as usual.

The equations are closed by the equation of state and constitutive relations for the coefficient of viscosity and the conductivity. The ideal-gas equation of state was used with the specific-heat ratio of 1.4 for air. The coefficients of viscosity in the above equations are obtained from Sutherland's law. The conductivity is obtained by assuming a constant Prandtl number ($Pr = 0.72$ for air).

Based on the finite-volume method, the governing equations can be described for a finite volume with an enclosing surface. It can thus be expressed in terms of the changes in the average state $\boldsymbol{U}$ in the finite volume,[9,10] and the surface integral becomes a sum of the fluxes over the six faces of a hexahedron. Consequently, Eq. (1) can be written in the normal flux form as

$$\Delta \tilde{V} \frac{\mathrm{d}\bar{\boldsymbol{U}}}{\mathrm{d}t} + \sum_{n=1}^{6} \boldsymbol{F}_n \, \Delta A_n = \boldsymbol{0} \tag{2}$$

where $\boldsymbol{F}_n$ is the flux normal to the cell surface, $\boldsymbol{F}_n = \bar{\boldsymbol{F}} \cos\alpha + \bar{\boldsymbol{G}} \cos\beta + \bar{\boldsymbol{H}} \cos\gamma$, with $\cos\alpha, \cos\beta$, and $\cos\gamma$ the direction cosines of the nth face.

Boundary Conditions

At the solid wall boundary of the inlet, the normal velocity is set equal to zero, since no mass or other convective flux can penetrate the wall. The other variables at the wall, e.g., pressure, velocity, and temperature, have to be determined by extrapolation from the interior of computational region to the boundary; then the fluxes at the wall can be evaluated.

In the far field a characteristic analysis based on the Riemann invariant is used to determine the values of the flow variable on the outer boundary of the grid. This analysis correctly accounts for wave propagation in the far field, which is important for achieving rapid convergence to a steady state.

Numerical Methods

The use of upwind difference schemes for solving the Euler and Navier-Stokes equations is becoming popular for several reasons.[11,12] For example, upwind schemes have natural numerical dissipation, better stability properties, and more accurate results. Furthermore, if techniques such as multigrid strategies, vector and parallel architectures, and local grid refinement are to be used, then the explicit scheme is preferred. Consequently, the explicit multistage Roe's flux-difference splitting scheme,[11,13,14] which can be applied to the conservation law and accurately represents the boundary layer, is chosen as the particular upwind method used here.

Discretizing the conservative form of Eq. (1) is useful for analysis, and Eq. (1) can be rewritten as

$$\frac{\mathrm{d}\bar{\boldsymbol{U}}}{\mathrm{d}t} + \frac{1}{\Delta \tilde{V}} \sum_{n=1}^{6} \boldsymbol{F}_n \, \Delta A_n = \boldsymbol{0} \tag{3}$$

in which the flux vector $\boldsymbol{F}_n$ can be expressed as the sum of an inviscid and a viscous/conductive part:

$$\boldsymbol{F}_n = \boldsymbol{F}_n^i + \boldsymbol{F}_n^\mu \tag{4}$$

The inviscid fluxes are approximated through a flux splitting scheme (Roe's scheme), and the viscous fluxes through central differencing.

The basic method of inviscid-flux computation is essentially the same for both grid-aligned and grid-independent schemes. It is based on Roe's approximated Riemann solver[15] for the Euler equations. The modified absolute velocities enforce the entropy condition, which eliminates expansion shocks and insures a smooth transition from subsonic to supersonic flow.

High-Resolution Scheme

In this paper a first-order scheme is initially applied, so the left and right states are chosen to be the cell average values to the left and right of the cell faces. In a high-resolution scheme, in order to raise the order of accuracy of upwind differencing, all one needs to do is to raise the order of accuracy of the initial-value interpolation that yields the zone-boundary data. Such schemes are called high-resolution schemes as opposed to total-variation-diminishing schemes, and they completely eliminate spurious oscillations when applied to one-dimensional nonlinear hyperbolic conservation laws and linear hyperbolic systems. The van Leer kappa scheme, in which the kappa number is one-third, was selected to obtain high-resolution upwind differencing.[16–19]

An optimal multistage scheme is used for the time integration; the multistage coefficients are modified according to Tai[12] and redefined using the Courant number for multidimensional use. Also, a residual smoothing method is imposed to accelerate convergence and improve numerical stability.

Turbulence Models

In this section the turbulence models used in the present study are described.

A. Baldwin-Lomax Algebraic Turbulence Model

In the algebraic turbulence model, the effects of turbulence are simulated in terms of an eddy viscosity coefficient μ_t. Thus, in the stress terms of the laminar Navier-Stokes equations, the molecular coefficient of viscosity μ is replaced by $\mu_{lam} + \mu_t$. The model avoids the necessity for finding the edge of the boundary layer, but it seems that it cannot simulate the separated-flow regions properly, and only provides satisfactory results for simple flow geometries.

B. Mitcheltree One-Equation Turbulence Model

This one-equation model was motivated by the success of the Johnson-King model,[20] has been developed from the available experimental observations on both attached and separated turbulent flows, and is based on a simplified version of the turbulent kinetic energy equation. It consists of three elements: an attached-flow formulation, a separated-flow formulation, and an automatic blending function that smoothly switches between the two formulations. The model does not require prior knowledge of the separation or its location.

C. Launder-Sharma Two-Equation Turbulence Model

In the present work, the Launder-Sharma k-ε model is used, because it does not require knowledge of the grid-point distance from the solid boundaries. The values of the eddy viscosity and eddy conductivity are estimated by solving two transport equations for the turbulent kinetic energy k and its dissipation rate ε. There is no substantial Reynolds-number restriction, since the turbulence closure used is well adapted to transitional flows as well as fully turbulent ones. For higher Mach-number values, the effects of compressibility on turbulence become dependent upon the density fluctuations. Therefore, this model is restricted to the Mach-number

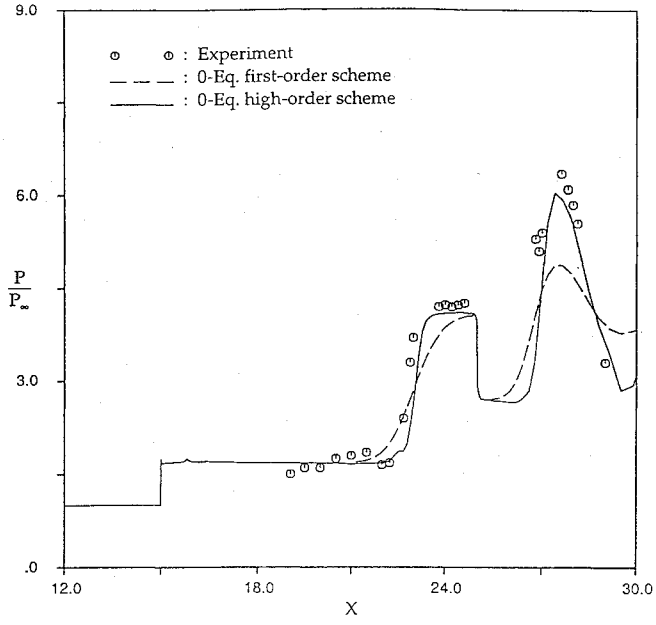

Fig. 4 Comparison of cowl surface pressure distributions for first- and high-order schemes at $M_\infty = 3.51$.

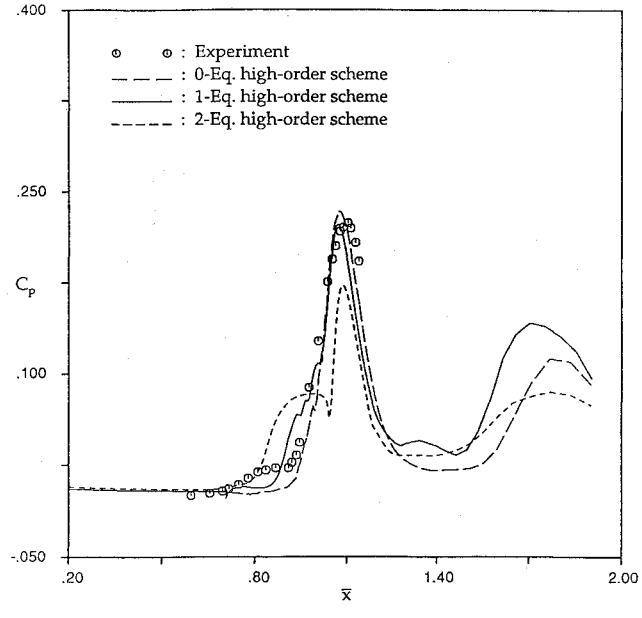

Fig. 3 Comparison of surface pressure distributions for two-dimensional plate at $M_\infty = 1.43$.

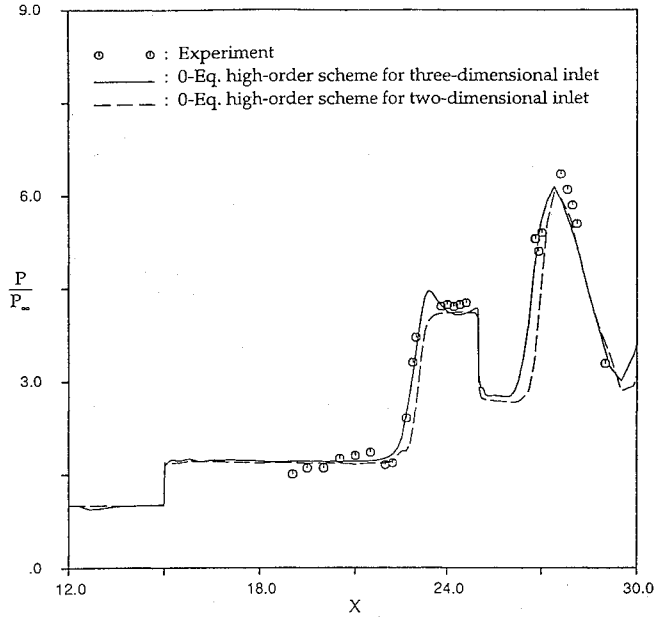

Fig. 5 Comparison of cowl surface pressure distributions for two- and three-dimensional inlets at $M_\infty = 3.51$.

range from $M = 0$ to $M = 5$, and is unable to predict some well-documented features of simple shear flows.

Results and Discussion

In this paper, the two-dimensional plate flowfield is calculated at freestream conditions of $M_\infty = 1.43$ and $Re = 9.0 \times 10^5$. The three-dimensional mixed compression inlet flowfield was analyzed at freestream conditions of $M_\infty = 3.51$ and $Re = 6.6 \times 10^6$. The computational results are summarized as follows.

A. Two-Dimensional Shock Impingement on a Flat Plate

The computed surface pressure-coefficient distribution along the flat plate is displayed in Fig. 3, together with the experimental data. At this flow condition, the shock wave penetrates the boundary layer, and flow separation takes place. Comparing the results with the experimental data,[21] we see that Mitcheltree's one-equation model is more reliable than the others, and good accuracy can also be obtained by using this model.

B. Two-Dimensional and Three-Dimensional Mixed Compression Inlet

Figure 4 shows the cowl pressure distribution. For the turbulent-flow computations the Baldwin-Lomax model is applied to analyze the two-dimensional inlet flowfield together with first-order and high-order schemes. In comparison with experimental results,[22] the high-order results are better than the first-order ones. In this paper,

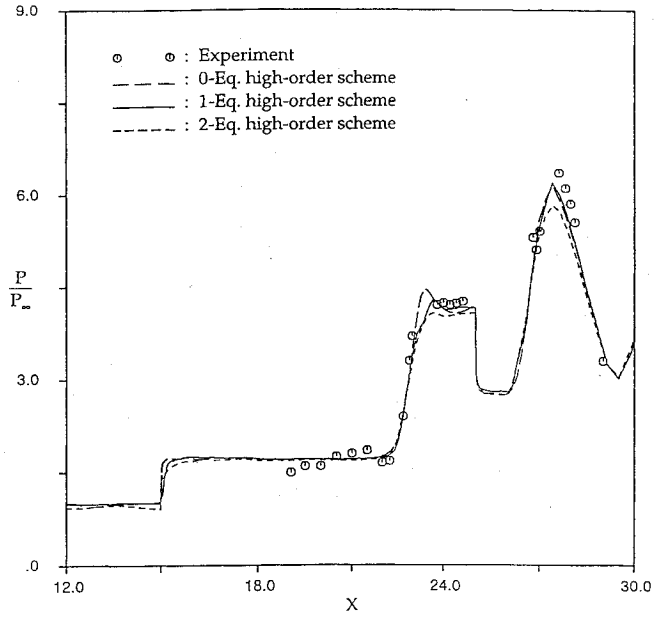

Fig. 6 Comparison of cowl surface pressure distributions for different turbulent models at $M_\infty = 3.51$.

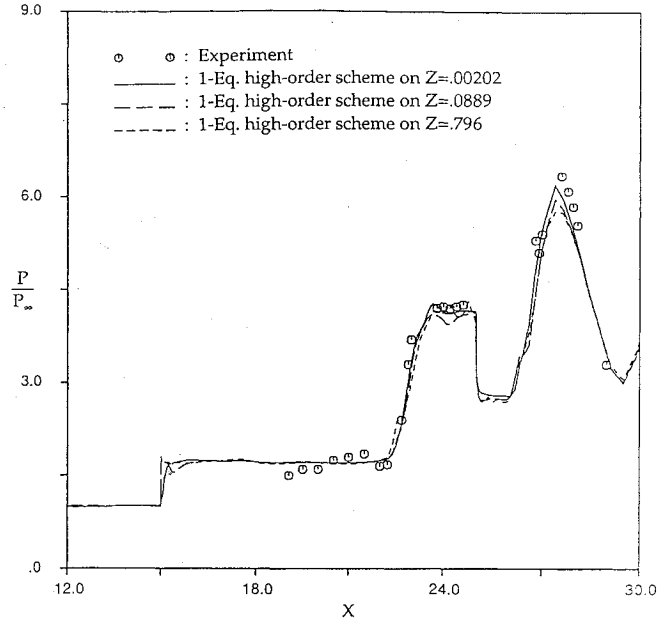

Fig. 7 Comparison of cowl surface pressure distributions at different distances from the wall at $M_\infty = 3.51$.

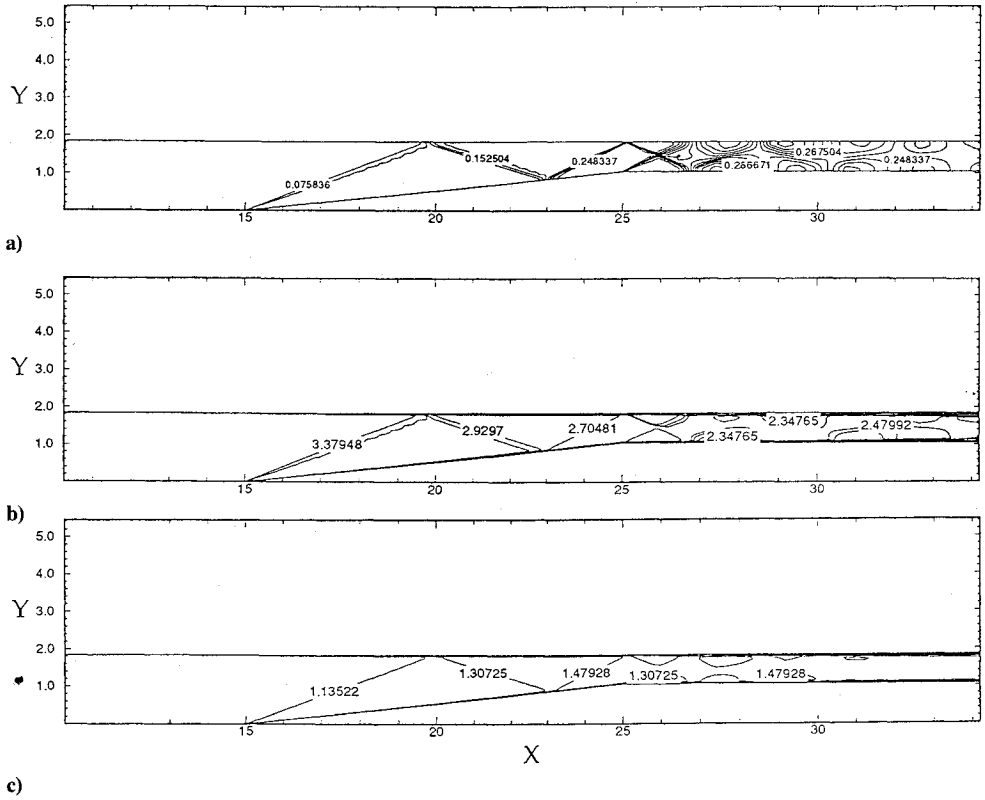

Fig. 8 Contours on x-y plane near wall at $M_\infty = 3.51$: a) pressure contours $P/\rho_\infty V_\infty^2$, b) Mach contours, and c) temperature contours T/T_∞.

simulating the inlet flowfield with a high-resolution scheme is thus considered appropriate.

Many computations on separated turbulent flows have been directed towards solving the two-dimensional, strong-impinging-shock interaction problem. The benchmark experimental flow of Knight[22] is three-dimensional; thus the elimination of three-dimensional effects must be considered. The cowl surface pressure distributions obtained from the experimental and computational results are shown in Fig. 5. The intersection of the oblique shock-wave train with the cowl at $X = 23$ and 27 in. is indicated by the sharp pressure rise in the vicinity of these locations. The cowl pressure computed is lower for two-dimensional calculations. The pressure obtained by three-dimensional computations is in good agreement with the experiment.

In Fig. 6, a comparison of cowl surface pressure distributions is made for different turbulence models at $M_\infty = 3.51$. The agreement upstream of the first shock impingment point is very good, but the pressure distributions between the first and second shock impingement points on the cowl are less accurate. However, Mitcheltree's one-equation model is more reliable than the others, and good accuracy can also be obtained by using this model in the high-speed inlet flowfield.

A comparison of cowl surface pressure distributions at different distances from the wall is shown in Fig. 7. The shock is stronger near the wall ($Z = 0.00202$ in.) than at the shock impingment point on the cowl. This is due to the wall effects in the experimental flowfield.

Figures 8a–8c show the Mach-number contours, pressure contours, and temperature contours, respectively, over the inlet flowfield $M_\infty = 3.51$ and $Re = 6.6 \times 10^6$. It clearly shows the location of the shock impingment point on the cowl, which is important information in predicting inlet performance.

Conclusions

A set of user-oriented computer programs have been developed that provide accurate and efficient computation of the inlet flowfield. The Reynolds-averaged Navier-Stokes equations were solved using an explicit multistage upwind flux-difference split scheme (Roe's scheme) coupled with different turbulence models.

The results show that the wall effects in a real three-dimensional flowfield must be considered and a high-resolution scheme is appropriate to simulate the inlet flowfield. The Mitcheltree one-equation turbulence model is superior to the others in this paper, as it predicts shock location and strength closer to the experimentally observed values than either the algebraic or the two-equation model. Good accuracy can also be obtained by using this model in the high-speed inlet flowfield.

Acknowledgment

The authors are grateful to the National Science Council of the Republic of China for financial support under Contract NSC 82-0401-D014-003.

References

[1]Ferziger, J. H., "Simulation of Incompressible Turbulent Flows," *Journal of Computational Physics*, 1987, pp. 1–48.

[2]Sorensen, V. L., "Computer Program for Calculating Flow Fields in Supersonic Inlets," NASA-TND-2897, July 1965.

[3]Vadyak, J., and Hoffman, J. D., "Calculation of the Flow Field Including Boundary Layer Effects for Supersonic Mixed-Compression Inlets at Angle of Attack," NASA-CR 167941, July 1982.

[4]Darian, A., and Daso, E. O., "Analysis of Shock Interactions and Flow Structure in High Speed Inlets," AIAA Paper 90-2132, July 1990.

[5]Baldwin, B. S., and Lomax, H., "Thin Layer Approximation and Algebraic Model for Separated Turbulent Flows," AIAA Paper 78-257, 1978.

[6]Mitcheltree, R. A., Salas, M. D., and Hassan, H. A., "One-Equation Turbulence Model for Transonic Airfoil Flows," *AIAA Journal*, Vol. 28, No. 9, 1990, pp. 1625–1632.

[7]Launder, B. E., and Sharma, B. I., "Application of the Energy Dissipation Model of Turbulence to the Calculation of Flows Near a Spinning Disk," *Letters in Heat and Mass Transfer*, Vol. 1, 1974, pp. 131–138.

[8]Anderson, D. A., Tannehill, J. C., and Pletcher, R. H., *Computational Fluid Mechanics and Heat Transfer*, New York, 1984, pp. 247–252.

[9]Abgrall, R.,"Generalization of the Roe Scheme for Calculating Flow of Mixtures of Variable Concentrations," *La Recherche Aerospatiale*, No. 1988-6, June 1988, French and English Edition, pp. 32–43.

[10]Schmidt, J. W., and Turkel, E., "Numerical Solution of the Euler Equations by a Finite-Volume Method Using Runge-Kutta Time-Stepping Schemes," AIAA Paper 81-1259, 1981.

[11]Roe, P. L., "Approximate Riemann Solvers, Parameter Vector, and Difference Schemes," *Journal of Computational Physics*, Vol. 43, 1981, pp. 357–372.

[12]van Leer, B., Tai, C. H., and Powell, K., "Design of Optimally Smoothing Multi-stage Schemes for the Euler Equations," *Proceedings of AIAA 9th Computational Fluid Dynamics Conference*, AIAA, Washington, DC, 1989, pp. 98–193.

[13]van Leer, B., Thomas, J. L., Roe, P. L., and Newsome, R. W., "A Comparison of Numerical Flux Formulas for the Euler and Navier-Stokes Equations," AIAA Paper 87-1104, 1987.

[14]Hirsch, C., "Numerical Computation of Internal and External Flow," Wiley-Interscience, New York, Vol. 2, 1989, pp. 460–469.

[15]van Leer, B., "Upwind-Difference Methods for Aerodynamic Problems Governed by the Euler Equations," *Large-Scale Computations in Fluid Mechanics*, Lectures in Applied Mathematics, Vol. 22, American Mathematical Society, Providence, 1985, pp. 327–336.

[16]van Leer, B., "Upwind-Difference Methods for Aerodynamic Problems Governed by the Euler Equations," *Proceedings of Large-Scale Computations in Fluid Mechanics*, Lectures in Applied Mathematics, Vol. 22, American Mathematical Society, Providence, RI, 1985, pp. 327–336.

[17]Mulder, W., and van Leer, B., "Experiments with Implicit Upwind Methods for the Euler Equations," *Journal of Computational Physics*, Vol. 59, 1985, pp. 232–246.

[18]van Albada, G. D., van Leer, B., and Roberts, J. W. W., "A Comparative Study of Computational Methods in Cosmic Gas Dynamics," *Astronomy and Astrophysics*, Vol. 108, 1982.

[19]Fromm, E., "A method for reducing dispersion in convective difference scheme," *Journal of Computational Physics*, Vol. 3, 1968.

[20]Johnson, D. A., and King, L. S., "A Mathematically Simple Turbulence Closure Model for Attached and Separated Turbulent Boundary-Layers," *AIAA Journal*, Vol. 23, No. 11, 1985, pp. 1685–1692.

[21]Liepmann, H. W., Roshko, A., and Dhawan, S., "On Reflection of Shock Waves From Boundary Layers," National Advisory Committee For Aeronautics, Rept. 1100, 1952.

[22]Kinght, D. D., "Calculation of High Speed Inlet Flows Using the Navier-Stokes Equations," Air Force Flight Dynamics Lab., Rept. AFFDL-TR-79-3138, Vol. 1, Feb. 1980.